Available online at www.sciencedirect.com
SCIENCE DIRECT
International Journal of Multiphase Flow 32 (2006) 677–691
International Journal of Multiphase Flow
www.elsevier.com/locate/ijmulflow

Spontaneous radial capillary impregnation across a bank of aligned micro-cylinders. Part II: Experimental investigations

V. Neacsu [a], A. Abu Obaid [b], S.G. Advani [a,b,*]

[a] Department of Mechanical Engineering, University of Delaware, 126 SPL, Newark, DE 19716, USA
[b] Center for Composite Materials, University of Delaware, 201 CCM, Newark, DE 19716, USA

Received 29 August 2005; received in revised form 7 February 2006

Abstract

This paper presents an experimental approach to study the capillary impregnation of a liquid across an array of parallel micro-cylinders. The technique presented successfully validates the theoretical findings of part I, and provides a methodology to calculate the fill time and the overall capillary impregnation dynamics for any arbitrary cylindrical sample made of aligned micro-cylinders, by taking into account the role of the trapped gas, which opposes and slows down the inward capillary flow.

Keywords: Multiphase flows; Flow through porous media; Capillary flow; Experimental technique; Micro-scale phenomena

1. Introduction

Numerous studies on capillary driven flows unveiled the main factors on which this phenomenon depends. Results for one-dimensional capillary driven flow were published early by Lucas (1918) and Washburn (1921) and applications to many types of geometries and specific problems were carried out. The particular case of capillary flow across a bank of aligned micro-cylinders was approached via analytical (e.g. Bernet et al., 1999; Foley and Gillespie, 2005; Pillai and Advani, 1995; Potter, 1997), numerical (Bayramli and Powell, 1990; Dimitrovova and Advani, 2002; Pillai and Advani, 1995; Young, 2004) and experimental techniques (Batch et al., 1996; Chwastiak, 1971; Foley and Gillespie, 2005, Pillai and Advani, 1996).

The experimental approach presented in this paper validates the theoretical results proposed in Part I for spontaneous capillary infiltration of a cylindrical porous structure, made of aligned micro-cylinders. It also sheds light on how gas displacement/dissolution are affected by material and process parameters.

* Corresponding author. Tel.: +1 302 831 8975; fax: +1 302 831 3619.
E-mail address: advani@me.udel.edu (S.G. Advani).

0301-9322/$ - see front matter © 2006 Elsevier Ltd. All rights reserved.
doi:10.1016/j.ijmultiphaseflow.2006.02.015

2. Background

Capillary transverse impregnation of a bank of aligned micro-cylinders is encountered in liquid composite manufacturing (LCM) processes. A common feature of this class of manufacturing procedures is that a porous material (preform) is placed in a closed mold cavity and then impregnated with a resin system. A series of chemical reactions solidify the resin and create a composite part.

The porous preform generally consists of woven or stitched bundles (tows) of cylindrical fibers. Each fiber is a few microns in diameter. The bundles hold together thousands of individual fibers and are usually a few millimeters in diameter. During the preform impregnation stage, resin fills the empty spaces between the bundles and then radially ingresses into the spaces between individual fibers in the bundles, at the same time displacing the air which exists in the empty pores. The mechanical properties of the end composite part significantly depend on how complete is the degree of preform saturation. To assist in this purpose, an imposed pressure difference is usually applied, by either pushing the resin with a positive pressure difference or pulling it through the preform by applying vacuum in at least one region of the mold. At the fiber scale level, it is the capillary pressure that helps infuse the bundles.

Previous experimental approaches reviewed derived results pertaining to the micro-flow (permeability and capillary pressure) either by visualizing the macro flow front through a transparent mold (Amico and Lekakou, 2001), or by monitoring the weight of liquid impregnated in a fibrous porous structure versus time (Foley and Gillespie, 2005; Chwastiak, 1971; Batch et al., 1996), approach based on the Wilhelmy principle. There are several challenging aspects which are revealed when one reviews the previous experimental studies. The list below enumerates those issues, and briefly describes how this paper addresses them.

A. In all previous experimental studies, the flow was linear one-dimensional, either in the direction of aligned fibers or perpendicular to their direction. Our paper investigates radial capillary flow within cylindrical fibrous porous samples. The flow is two-dimensional, as the flow front advances inward as a quasi-cylindrical surface of decreasing diameter.

B. Another issue is related to the fact that previous experimental studies approximate the capillary pressure with different theoretical models. Laplace equation (Eq. (1)) is the basis of these approximating models:

$$p_c = \sigma \cdot \left(\frac{1}{r_{c_1}} + \frac{1}{r_{c_2}} \right) \tag{1}$$

where σ is the liquid surface tension, and r_{c_1} and r_{c_2} are the principal radii of curvature of the meniscus interface.

However, the approximations proposed for capillary pressure (e.g. Bayramli and Powell, 1990; Ahn et al., 1991; Foley and Gillespie, 2005) yield different numerical results, for the same set of material and process parameters. Our experimental study validates the expression of the mean capillary pressure proposed in Part I in which the instantaneous capillary pressure proposed by Bayramli and Powell (1990) was averaged after taking into consideration the physics of the capillary impregnation process more appropriately.

C. Little has been done in the previous experimental studies to address the issue of how the presence of air between the fibers affects the dynamics of the capillary flow through the fiber bundles. This paper shows how significant the opposing effect of entrapped air is at various fiber volume fractions and at various levels of liquid pressure around the fiber bundle.

3. Experimental approach

Our experimental investigation was based on monitoring the capillary flow through a cylindrical porous sample, made of aligned fibers (Fig. 1). Hand-made sensors were placed inside the sample to detect the arrival times of the impregnating liquid at the sensors' locations. In order to minimize flow in longitudinal direction and force the flow to develop primarily in the radial direction toward the center of the fiber bundle, the ends of the samples were sealed with epoxy resin before the experiment.

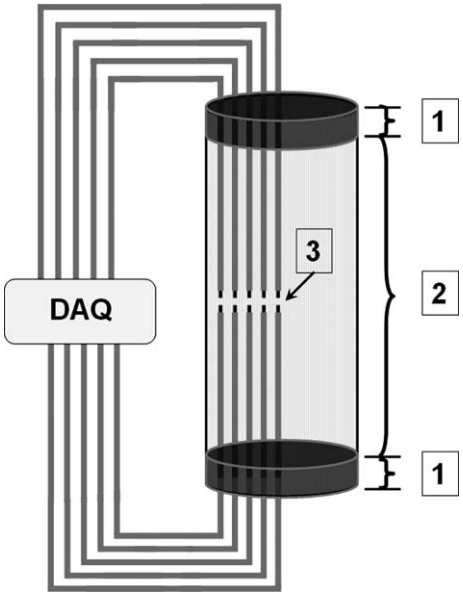

Fig. 1. Sketch of the setup used to detect the liquid arrival times with sensors at radial locations [3] in the transversal mid-plane. The cylindrical porous sample was sealed at the ends with epoxy resin [1], in order to minimize flow in the longitudinal direction in between the aligned fibers [2].

The test consisted of immersing the sample in a liquid, with no imposed pressure difference to assist the flow. We consider the flow primarily driven by the capillary pressure, although hydrostatic pressure effects are certainly present. We neglected the effect of hydrostatic pressure, which we estimated as up to one order of magnitude lower than average capillary pressure. Most of the tests were run at atmospheric pressure, but some were conducted with the setup enclosed in a chamber subjected to a lesser pressure than the atmospheric pressure.

3.1. Sample description

Our study used two types of samples, designed as enlarged replicas of real fiber yarns from fabrics used in composite manufacturing. Both types of samples were made of aligned E-Glass fibers manufactured by Owens Corning, averaging 16 μm in diameter. The only difference between the two types of samples is that one included a tube with perforations at the center. The samples with the tube at the center (named 'hollow samples' herein, and depicted in Fig. 2) were used either for the purpose of generating the dependence of permeability on fiber volume fraction, or for simulating radial capillary impregnation with no back pressure being exerted as the air could escape through the uniformly distributed perforations of the tube. The other 'full samples' were bundles without any tube in the center so the air is either entrapped or can escape only by dissolution in the impregnating liquid. The samples were made by aligning same-length yarns and tying them together using wire rings, in such a way that a cylindrical porous structure of circular cross-section is created. Before the wire rings were completely tightened, one to five sensors were also inserted in longitudinal direction, parallel to the fibers, at various radial locations, spaced as evenly as practically possible.

The aspect ratio choice took the following into consideration:

- The sample had to be sufficiently thick to allow for several sensors to be placed in radial direction from the center of the sample to its outside circumference, but at the same time the sample had to be thin enough to reduce irregularities in fiber distribution in radial direction.
- The sample had to be sufficiently long to avoid end effects due to imperfect sealed ends, but at the same time it had to be short enough to avoid significant variations of sample diameter in longitudinal direction, as well as the occurrence of longitudinal flow.

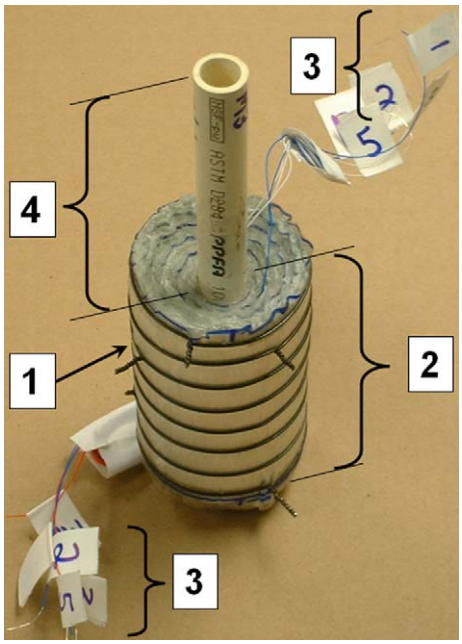

Fig. 2. Hollow sample in the making, before the ends were sealed with epoxy resin. Circumferential wire rings (1) were used to tie together aligned fibers (2), after five sensors (3) were inserted at the desired radial locations. In the case of hollow samples, an inner tube (4) was placed at the center of the porous sample. The inside part of the tube had been perforated to allow for flow of air and liquid. The sample shown is 60 mm in diameter and features a fiber volume fraction of 62%. The outer diameter of the inner tube is 16 mm.

3.2. Sensors

It is necessary to specify that the devices we used to monitor the flow, although named 'sensors' throughout the papers, are simple electric circuits made of copper wrapping wire of 250 μm diameter, electrically insulated by a plastic coating. Initially, each electric circuit was open, due to a 1–2 mm discontinuity purposely created in the wire (Fig. 3). A simple contact resistance circuit-based (CRC) setup was created, by connecting in series a resistance R, a constant power supply V_{ps}, and the sensor resistance R_s. When the liquid reaches the sensor gap, the sensor resistance R_s drops suddenly from infinity (value for the open circuit) to a finite value depending on the electro-chemical properties of the impregnating liquid. Consequently, the data acquisition system measures a non-zero value of the real time voltage across the resistance R, as given by $V = V_{ps} \cdot (1 + R_s/R)^{-1}$.

The data acquisition system excited the circuits individually, and therefore detected the closure of each electric circuit, at the moment when liquid arrived at the specific location (Fig. 4).

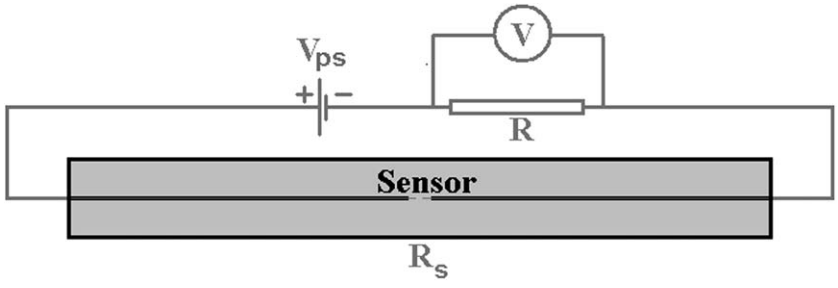

Fig. 3. Schematic of one individual circuit excited by the data acquisition system.

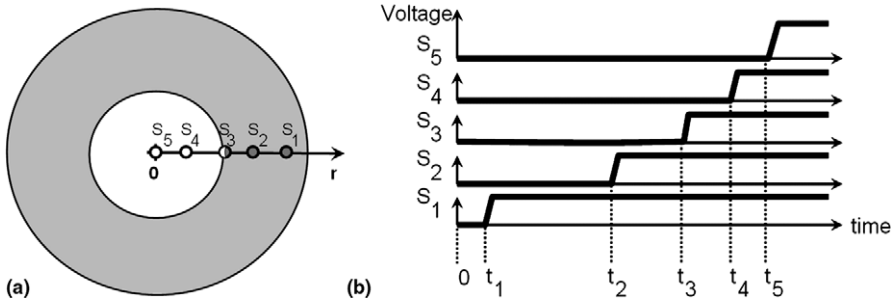

Fig. 4. (a) Sensors location in radial direction, shown in a cross-sectional view through the mid-plane of a full sample. The grey area corresponds to the already wetted porous medium, whereas white indicates the inside region which is still dry. (b) Sketch of the signals read from the sensor circuits by the data acquisition system.

Thus, 'sensor locations' designate the millimeter-size regions around the gaps, which were all situated in the transversal mid-plane of the cylindrical sample (see Fig. 1). Because the insertion of the sensors was done manually, relative errors of around 3–5% were associated with the exact location of the sensors.

Unlike the full samples, the sensors used inside hollow samples were spaced from the outside of the inner perforated tube to the outside of the porous sample. In the tests on hollow samples, the last arrival time recorded was the one corresponding to the inner-most sensor, located on the outer side of the perforated tube.

3.3. Preliminary parameters

Viscosity of the liquid was measured using a Brookfield® DV-E viscometer. Density of the fiber material ρ_f, was calculated from buoyancy consideration, as follows:

$$\rho_f = \rho_w \cdot \frac{w_a}{w_a - w_w} \tag{2}$$

where w_w is the apparent weight of the measuring sample immersed into distilled water, w_a is the actual weight of the measuring sample in air, and ρ_w is the water density.

The surface tension of the impregnating liquid and the advancing contact angle were measured with a Cahn® DCA 322 Dynamic Contact Angle Analyzer.

Average fiber diameters were measured by two techniques, which gave comparable results. First, several fibers were photographed under a Metallux 3 microscope and the diameters in the pictures were measured using image processing software (Image Pro). Second, the microbalance of the Cahn® DCA 322 Dynamic Contact Angle Analyzer was used to weigh fiber of a known combined length. The density was calculated as the ratio between the measured weight and the calculated volume of the combined micro-rod.

Fiber volume fraction was approximated after measuring the average cross-sectional area of the sample, knowing how much material was tied together to make the sample (linear density of sample):

$$V_f = \frac{\rho_l}{\rho_f \cdot A_s} \tag{3}$$

where ρ_f is the density of the fiber material (glass) and ρ_l is the linear density of the fiber material used to make the sample. A_s is the average cross-sectional area of the sample, which applies only to the area occupied by fibers; naturally, the cross-sectional area A_s of hollow samples excluded the cross-section of the inner perforated tube.

3.3.1. Permeability

Preliminary experimental measurements of transverse permeability were performed on hollow samples, to generate the dependence of permeability on the fiber volume fraction. In order to do so, hollow samples similar to the one depicted in Fig. 2 were used, with the only exception that sensors were not inserted in them. The samples were immersed into a bath of liquid placed on a scale connected to a data acquisition system, and

vacuum was used to draw liquid through the sample and through the inner perforated tube. The continuous acquisition of data from the scale indirectly allowed for the calculation of the steady mass flow rate through the porous sample. This was done after the sample was fully saturated with liquid. The following equation (Washburn, 1921) allowed us to calculate the transverse permeability, since all the right-hand side parameters were known:

$$K = \frac{Q \cdot \eta}{2\pi L \cdot \Delta p} \cdot \ln\left(\frac{R_0}{R_{\text{in}}}\right) \tag{4}$$

where Q is the volume flow rate, η is the liquid viscosity, Δp the applied pressure difference, L is the effective length of the cylindrical porous sample, R_0 is the outside diameter of the sample and R_{in} is the outside diameter of the inner perforated tube.

The volume flow rate was calculated from the mass flow rate, as

$$Q = \frac{1}{\rho} \cdot \frac{\mathrm{d}m}{\mathrm{d}t} \tag{5}$$

where ρ is the density of the testing liquid, and $\mathrm{d}m/\mathrm{d}t$ is the mass flow rate.

A typical experimental determination of the mass flow rate through a hollow sample is shown in Fig. 5. The plot shows a linear decrease of the mass recorded by the scale on which the bath containing the sample and liquid was placed. Data acquired during the first 2.5 h (before the linear trend was observed) were discarded, as they corresponded to a pre-saturation filling stage.

For the purpose of the representative test shown in Fig. 5, water was used (viscosity was 0.001 Pa s), the level of applied vacuum was 80 kPa (−23.6 in Hg), and the sample featured a fiber volume fraction of 66%, outer diameter of 56 mm, length of 87 mm, with an inner perforated tube of 15.8 mm in diameter. The mass flow rate was approximated as equal to the slope of the linear trend, equal to 5.3 mg/s. Eq. (4) led to a value of the transverse permeability of 1.5×10^{-16} m^2. A series of 11 similar tests were conducted to generate a Kozeny–Carman (Carman, 1937) curve fit to describe transverse permeability as a function of fiber volume fraction, in the range of [59–72%]. The experimental results indicated a correlation coefficient of −0.81 (inverse correlation) between the normalized permeability (K/r_{f}^2) and the fiber volume fraction

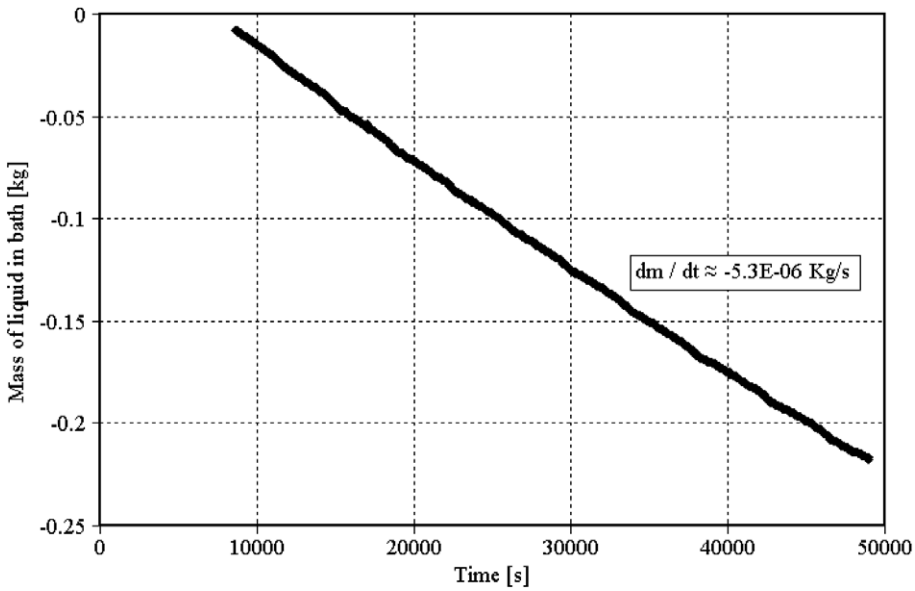

Fig. 5. Representative measurement of mass flow rate through a hollow porous sample, which allows one to calculate the transverse permeability.

(V_f). The transverse permeability was approximated using the following empirical equation, whose coefficient was obtained using the least square fitting technique:

$$\frac{K}{r_f^2} = 3.08 \times 10^{-4} \cdot \frac{(1 - V_f)^3}{V_f^2} \tag{6}$$

where r_f is the fiber radius and V_f is the fiber volume fraction.

The relative scatter displayed by the experimental values of permeability can be justified by the fact that the geometry of the samples was far from the assumed uniform distribution of fibers within the porous preform. Commonly observed irregularities of these samples include:

- Non-uniform packing densities in longitudinal direction. Variations of the sample diameter in longitudinal direction were measured up to ±2%, causing variations of the fiber volume fraction of up to ±4% in longitudinal direction.
- Non-uniform packing densities in radial direction. Visual inspection of the cross-sections of several samples under a microscope indicated that the technique used to tie together the fibers into aligned porous cylindrical structures sometimes created a region of higher fiber volume fraction at the center of the sample and lower fiber volume fraction at the outside of the sample. Such variations of the local fiber volume fraction in radial direction amounted up to ±5%.

As a consequence of sample imperfections, it is not surprising that our empirical equation (6) yield much lower values than well-known approximating models derived for ideally uniform fiber distribution (Bruschke and Advani, 1993; Carman, 1937; Gebart, 1992). The technique to make samples was kept consistent throughout our experimental study and we used the average fiber volume fraction of a sample to predict its average transverse permeability, as expressed by Eq. (6).

3.3.2. Capillary pressure

The expression we use for the mean capillary pressure is the one proposed in Part I as a function of the liquid surface tension, advancing contact angle, fiber radius and average fiber volume fraction. The testing liquid used was a 2% volumetric solution of 3-glycidoxypropyl trimethoxysilane, which was chosen because it displays good capillary properties. This liquid had a viscosity equal to that of water of 10^{-3} Pa s and its measured surface tension was 0.053 N/m (±0.007 N/m). The measured advancing contact angle formed at the interface between the fiber used and the testing liquid was 15° with an error of ±3°. Use of more viscous liquids was avoided as the fill times would have been at least 2 orders of magnitude longer.

4. Results and discussion

4.1. Determination of arrival times

The arrival time of capillary flow front at a sensor location was recognized by the data acquisition system at the instant a voltage change is registered through the corresponding electric circuit. The results of a typical test on a full sample are shown in Fig. 6.

Because the sensors were made manually, the sizes of the gaps in the sensor circuits were not equal, and consequently the peak voltages read were not equal either. This is the reason why each voltage curve in Fig. 6 is normalized with respect to the maximum value read for each individual electric circuit. The obvious jump in voltage for each sensor makes it easy to identify the foot of the curve as the arrival time at the corresponding radial location. The times, along with the sensors locations are listed in Table 1.

4.2. Validation of analytical model

In order to validate the theoretical model proposed in Part I, a series of eight capillary impregnations of hollow samples where conducted. The objective of these experiments was that, unlike the real case in which

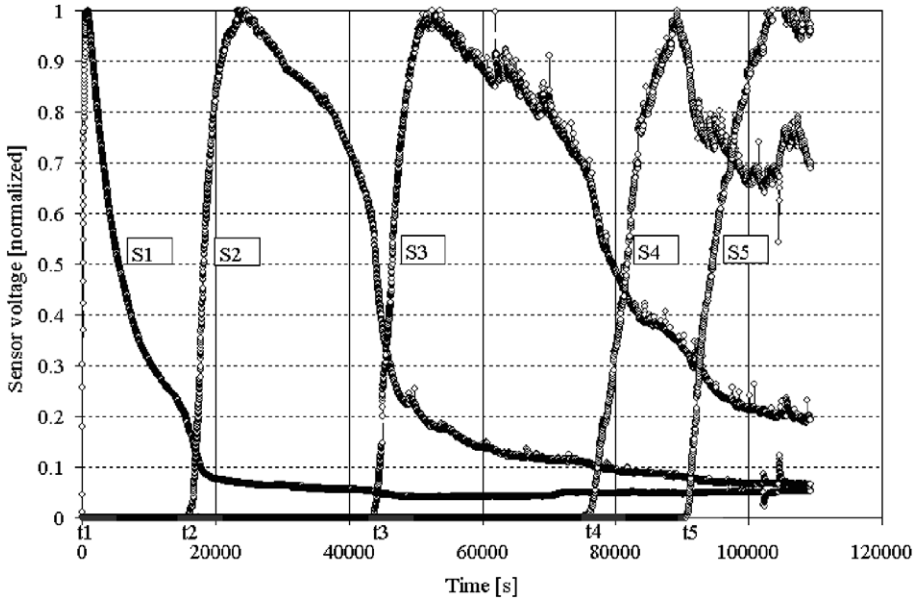

Fig. 6. Experimental reading of the signal in each sensor circuit, during a typical test. The arrival time of liquid at a sensor location was identified at the foot of the corresponding curve.

Table 1
Flow front arrival times at the sensors locations, for a representative full sample

	Flow front arrival time [s]	Sensor location (radius) [mm]
Start of test	0	23.4
Sensor 1	64	20.1
Sensor 2	16,960	14.4
Sensor 3	44,700	9.6
Sensor 4	77,500	5.1
Sensor 5	91,530	0.0

the entrapped air is compressed by the advancing flow front and slows down the flow, the specially made hollow samples would allow the air to escape through the inner perforated tube (Fig. 7). These experiments were designed in such a manner that they would allow one to verify the accuracy of the theoretical model to predict the real impregnation dynamics, in the simplified case where air does not play any role in the process. This specific case is a particularization of the general model presented in Part I, in which the one parameter describing the effect of air entrapment/dissolution (δ) is assigned a value of zero. This parameter δ as introduced in Part I is a weighing factor between two limiting situations of all air entrapped and no entrapped air. Parameter δ also determines the length and duration of the first stage of the capillary impregnation, during which air entrapment does not slow down the capillary impregnation.

The parameters of the eight tests run on hollow samples are presented in Table 2. The last column lists the ratios between the experimental fill times (arrival time of liquid at the inner-most sensor location) and theoretical estimation. In the simplified case which applies here, the total impregnation time for a hollow sample can be estimated as

$$t_f = \frac{R_0^2 \cdot \eta \cdot (1 - V_f)}{4K \cdot \overline{p_c}} [1 - \varepsilon_{in}^2 (1 - 2 \ln \varepsilon_{in})] \tag{7}$$

where η is the liquid viscosity, R_0 is the sample radius, V_f is the fiber volume fraction, K is the transverse permeability, $\overline{p_c}$ is the mean capillary pressure, and ε_{in} is the normalized radial location of the inner-most sensor, equal to the ratio between the radii of the inner tube and the sample ($\varepsilon_{in} = R_{tube}/R_0$).

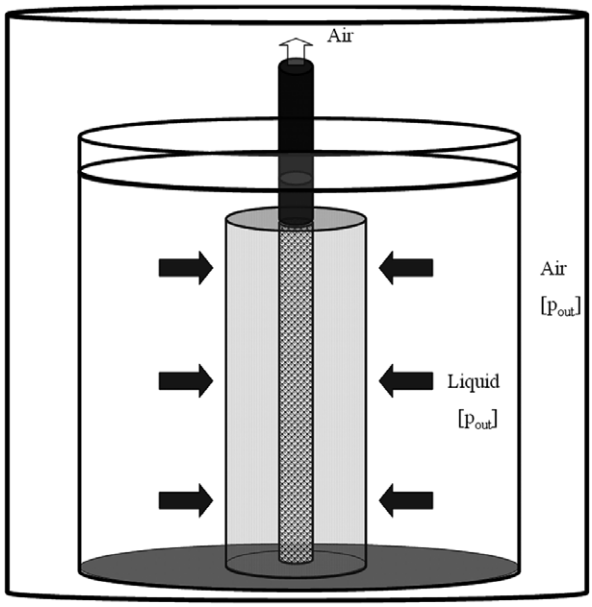

Fig. 7. Sketch of a capillary impregnation test on a hollow sample. Flow front advances radially and pushes the entrapped air through the inner perforated tube outside.

Knowing that these results may be significantly influenced by errors in preliminary parameters, such as permeability, we consider satisfactory the fact that the ratios obtained were all around unity, the average fill time ratio being 1.04, with a standard deviation of 14%.

It is important to notice that agreement between experiment and theory for the capillary impregnation of hollow samples was reached regardless of the outside pressure to which the setup was subjected (p_{out}). Fill time ratios were in the vicinity of unity for tests conducted either at atmospheric pressure ($p_{out} = 10^5$ Pa) or under vacuum ($p_{out} = 1.5 \times 10^4$ Pa).

Fig. 8 shows comparatively the relationship between flow front radial location and time, determined experimentally and calculated theoretically with the model developed in Part I for a representative hollow sample (hollow sample number 5, as per Table 2).

The good correlation between the experimental and theoretical fill times for hollow samples indicates that the estimations of the mean capillary pressure, as well as of the transverse permeability are reliable and can be further used in the study of full samples, where the role of air cannot be neglected.

4.3. Role of entrapped air on the dynamics of capillary radial impregnation

Similarly to the hollow samples, capillary impregnation tests were conducted on full samples. A typical set of experimental data (full sample number 13, as per Table 3) is presented in Fig. 9. It is interesting to note that the experimental arrival times in that case were much higher than what the theoretical model would estimate if the role of air is not taken into consideration (case $\delta = 0$). A numerical computer code was written to find the particular value of the parameter δ which generates the best curve fit for the experimental data, as described in Eqs. (12)–(14) of Part I. It is not surprising that the value of δ for this particular test was found very close to unity ($\delta = 0.96$), which indicates that the escape/dissolution of inside air through the impregnating liquid happens at a very slow rate greatly inhibiting the inward capillary advancement of the flow.

After collecting similar results for all 14 full samples tested (Table 3), we are able to show what role the air escape/dissolution process plays in the radial impregnation phenomenon, and how this depends on material and process parameters. For all full samples listed in Table 3, the fiber diameter was 15.6 μm, and all tests were run at atmospheric pressure. The sample diameters varied in a narrow interval, with an average of 50.2 mm, and a standard deviation of approximately 6%. Although the variation of fiber volume fraction from one

Table 2
Material and process parameters for the eight tests performed on hollow samples

	Fiber volume fraction [%]	Sample diameter [mm]	Inner tube diameter [mm]	Fiber diameter [μm]	Estimated transverse permeability [m^2]	External liquid pressure, p_{out} [Pa]	Mean capillary pressure [Pa]	Experimental fill time [s]	Theoretical fill time [s]	Fill time ratio [–]
1	61.5	59.9	15.8	15.6	2.8E−15	1.5E+04	8.5E+03	2556	2699	0.95
2	66.6	52.0	12.7	16.3	1.7E−15	1.5E+04	1.0E+04	2292	2405	0.95
3	70.3	56.4	15.8	15.6	9.9E−16	1.5E+04	1.0E+04	3691	4242	0.87
4	59.6	51.4	12.7	16.3	3.8E−15	1.0E+05	8.6E+03	1414	1551	0.91
5	66.0	57.9	15.8	15.6	1.7E−15	1.0E+05	9.3E+03	3540	3261	1.09
6	66.1	49.0	12.7	16.3	1.8E−15	1.0E+05	9.7E+03	2178	1956	1.11
7	70.5	46.3	12.7	16.3	1.1E−15	1.0E+05	1.1E+04	2848	2571	1.11
8	71.1	46.4	12.7	16.3	9.8E−16	1.0E+05	9.8E+03	2556	2971	1.30

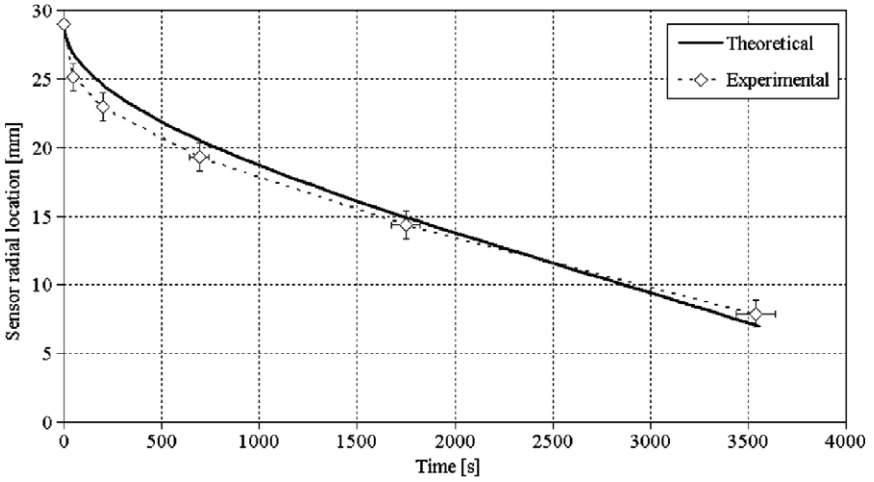

Fig. 8. Typical experimental dependence of sensor location versus time, in comparison to the theoretical variation of time versus flow front location, for a representative hollow sample.

Table 3
Material and process parameters for the tests performed on full samples

	Fiber volume fraction, V_f [%]	Sample diameter, $2R_0$ [mm]	Estimated transverse permeability, K [m^2]	Mean capillary pressure, $\overline{p_c}$ [Pa]	Experimental fill time, $t^{\delta}_{f\_experimental}$ [s]	Fill time ratio, τ_f [–]	Parameter δ [–]
1	48.0	56.0	1.1E−14	3.9E+03	3628	1.6	0.69
2	50.3	54.8	9.0E−15	6.8E+03	4396	3.0	0.72
3	51.0	54.0	8.4E−15	6.9E+03	4620	3.2	0.73
4	52.4	53.7	7.3E−15	7.1E+03	8873	5.4	0.84
5	56.4	51.9	4.9E−15	7.7E+03	13288	6.8	0.87
6	57.2	51.5	4.4E−15	7.8E+03	15306	7.5	0.88
7	61.4	49.5	2.8E−15	8.5E+03	23660	9.7	0.91
8	64.9	48.4	1.9E−15	9.1E+03	64780	22.0	0.96
9	66.7	47.7	1.6E−15	9.1E+03	49555	14.9	0.94
10	67.1	47.1	1.5E−15	9.3E+03	52803	15.9	0.94
11	67.6	47.3	1.4E−15	9.5E+03	60195	17.9	0.95
12	68.7	46.8	1.2E−15	9.8E+03	53060	14.9	0.94
13	69.5	46.7	1.1E−15	1.0E+04	91530	23.9	0.96
14	69.7	47.0	1.1E−15	1.0E+04	79450	20.4	0.95

sample to the next induced different values of transverse permeability and mean capillary pressure, each result (fill time ratio τ_f) was normalized with respect to the corresponding theoretical fill time, calculated for the ideal case $\delta = 0$:

$$\tau_f = \frac{t^{\delta}_{f\_experimental}}{t^{0}_{f\_theoretical}} \tag{8}$$

where $t^{\delta}_{f\_experimental}$ was the arrival time at the center sensor, measured during the actual test, and $t^{0}_{f\_theoretical}$ was the estimation of the fill time using the theoretical model, when air is not taken into consideration. The latter is given by the expression

$$t^{0}_{f\_theoretical} = \frac{R_0^2 \cdot \eta \cdot (1 - V_f)}{4K \cdot \overline{p_c}} \tag{9}$$

where all quantities are defined earlier.

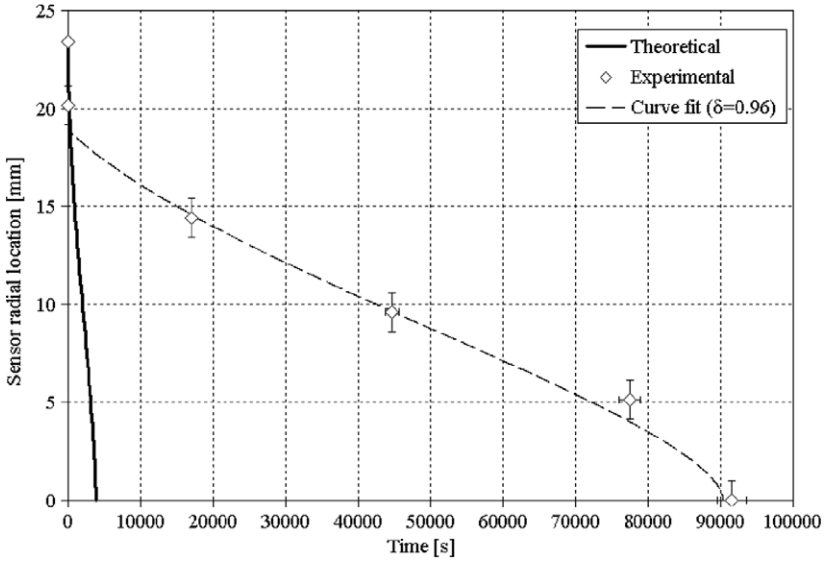

Fig. 9. Typical experimental dependence of time versus sensor location, in comparison to the theoretical variation of time versus flow front location, for a full sample. The thick continuous curve corresponds to the relationship between flow front location and time, in the ideal case where air did not play any role ($\delta = 0$). In reality, the experimental data match well the curve corresponding to a value of 0.96 for the scalar parameter δ.

Using data presented in Table 3, we could plot the variation of parameter δ as a function of fiber volume fraction V_f (see Fig. 10). It is remarkable that increasing fiber volume fraction V_f is associated with higher values of parameter δ, which indicate a more inhibiting role of the air escape/dissolution process, as far as the dynamics of the capillary impregnation is concerned. The results presented in Fig. 10 are for a range of fiber volume fractions from 45% to 70%, for which a quadratic trend was identified, approximated well with a R-squared value of 0.98, as

$$\delta \approx 0.9945 \cdot V_f^2 + 2.0524 \cdot V_f \tag{10}$$

The trend presented in Fig. 10 fits well the experimental data, to which two additional points were added. Leaving aside the pertinent aspect that capillary effects do not manifest at V_f approaching zero, point (0;0) should be on the fitting curve, based on the common sense assumption that at minimum fiber volume fraction, air should not have any influence on the impregnation dynamics (parameter $\delta = 0$). Similarly, one could argue that at maximum fiber volume fraction ($V_f \approx 90.7\%$ for hexagonal packing pattern), air presents its most opposing effect ($\delta = 1$), therefore point (0.907; 1) should also be used to generate the fitting curve.

It is important to underline that the trend described by empirical Eq. (10) was obtained under specific conditions of pressure and sample sizes, so caution should be used when applying it to other configurations. The

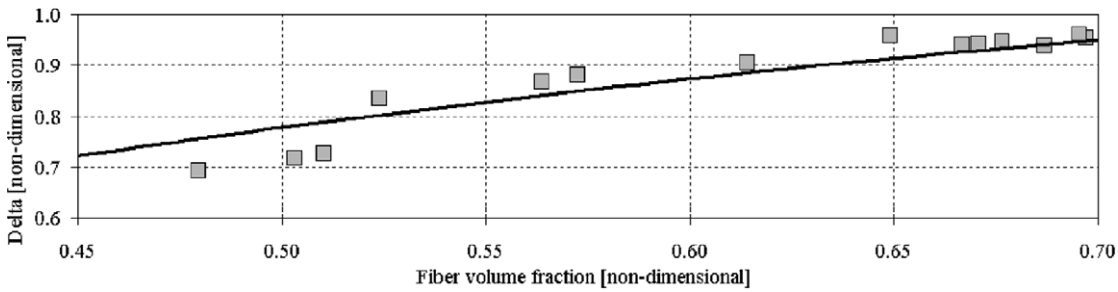

Fig. 10. Variation of parameter δ, versus fiber volume fraction V_f. The trend indicate that denser packing (higher V_f) causes higher values of parameter δ, which is equivalent to a more significant role played by the inside air, in opposing the capillary flow.

methodology we employed here demonstrates that it is possible to get insight into how the air dissolution process [parameter δ, and indirectly the fraction of escaped air $\lambda(\varepsilon)$] is influenced by material parameters, specifically, V_f.

Thus, one could use the model proposed in Part I to simulate the behavior of the capillary impregnation process, for any arbitrary new cases once the constitutive equation for parameter δ is determined.

An alternative way to analyze the results shown in Fig. 10 is to plot the variation of fill time ratios instead of parameter δ, versus the fiber volume fraction. The fill time ratios were calculated by scaling the experimental fill time (arrival time at the inner-most sensor) with respect to the theoretical value of fill time for the ideal case when no air is present or it can all escape unopposed ($\delta = 0$). Fig. 11 presents data for the same samples described in Table 3. Previously drawn conclusion is confirmed, that increasing fiber volume fractions increase the inhibiting role of air escape (increasing fill time ratios, increasing parameter δ).

To examine the role of external pressure on the air escape/dissolution, we plotted in Fig. 12 the fill time ratios for two sets of samples, featuring common parameters (as listed in Table 4), which were tested under different levels of external pressure. The tests were conducted in such a way that the setup was kept in an

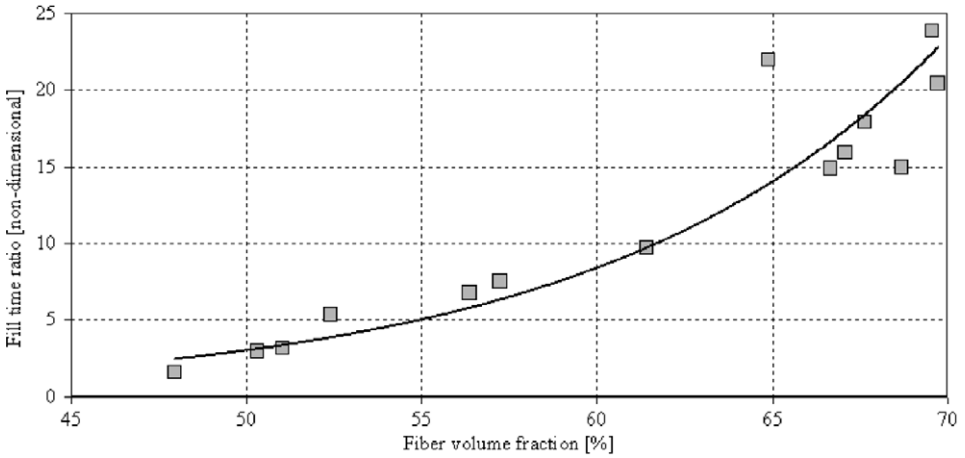

Fig. 11. Effect of fiber volume fraction on fill time ratios. Fill time ratios were calculated by normalizing the experimental fill times with respect to the theoretical predictions, in the case of air absence from the sample ($\delta = 0$).

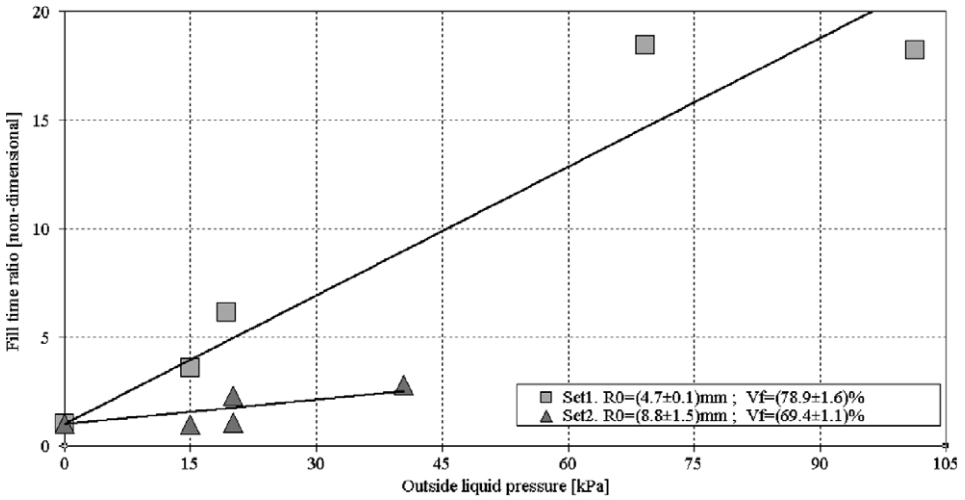

Fig. 12. Effect of external pressure p_{out} on fill time ratios, for two sets of similar full samples.

Table 4
Common parameters of full samples tested to reveal the role of outside pressure p_{out} on parameter δ

Set #	Sample diameter [mm]	Fiber volume fraction [%]
1	(9.4 ± 0.2)	(78.9 ± 1.6)
2	(17.6 ± 3.0)	(69.4 ± 1.1)

enclosure at constant pressure before and during the actual capillary impregnation (Fig. 7). Therefore, the initial value of air pressure was the same as the pressure external liquid pressure, constant during the test.

The reason the data in Fig. 12 were not processed in a manner compatible with Fig. 10 is because unlike for thick samples, thinner samples could not accommodate several sensors, which would not result in reliable values for δ. As a consequence, fill time ratio, rather than the factor δ was used to reflect the rate of air escape/dissolution.

Although relatively few samples were used to generate the results plotted in Fig. 12, it is still possible to identify quasi-linear trends indicating that higher external pressures do play an important role in the air escape/dissolution, by slowing down the impregnation process significantly. The opposite happens at lower outside pressures, which facilitate an easier escape of the entrapped air outward, resulting in a lower fill time ratio. This is not surprising, since due to the nature of the experiment, lower pressures are associated with a smaller quantity of entrapped air, to begin with. Also, the comparison between the two trendlines confirms that higher fiber volume fraction leads to a slower air escape/dissolution.

5. Conclusions

The experimental study presented in this paper validated the theoretical model proposed in Part I. Capillary impregnation tests conducted on hollow samples simulated the ideal case in which the air could escape without exerting any back pressure. This also verified the equations used to approximate the mean capillary pressure and the transverse permeability.

Tests conducted on full samples helped better understand the role of air entrapped and its dissolution, on the overall impregnation dynamics. A single parameter, δ was shown to account for the influence of the entrapped air. This parameter also shed light on the influence of external liquid pressure and fiber volume fraction on the ease with which the air could escape.

Acknowledgments

The authors acknowledge support of their work by the AMIPC grants N00014-02-1-0811 and N00014-03-1-0891.

References

Ahn, K.J., Seferis, J.C., Berg, J.C., 1991. Simultaneous measurements of permeability and capillary pressure of thermosetting matrices in woven fabric reinforcements. Polym. Compos. 12, 146–152.

Amico, S., Lekakou, C., 2001. An experimental study of the permeability and capillary pressure in resin-transfer moulding. Compos. Sci. Technol. 61, 1945–1959.

Batch, G.L., Chen, Y.-T., Macosko, C.W., 1996. Capillary impregnation of aligned fibrous beds: experiments and model. J. Reinf. Plast. Compos. 15, 1027–1051.

Bayramli, E., Powell, R.L., 1990. The normal (transverse) impregnation of liquids into axially oriented fiber bundles. J. Colloid Interf. Sci. 138, 346–353.

Bernet, N., Michaud, V., Bourban, P.-E., Månson, J.-A.E., 1999. An impregnation model for the consolidation of thermoplastic composites made from commingled yarns. J. Compos. Mater. 33, 751–772.

Bruschke, M.V., Advani, S.G., 1993. Flow of generalized Newtonian fluids across a periodic array of cylinders. J. Rheol. 37, 479–498.

Carman, P.C., 1937. Fluid flow through granular beds. Trans. Inst. Chem. Eng. 15, 150–167.

Chwastiak, S., 1971. A wicking method for measuring wetting properties of carbon yarns. J. Colloid Interf. Sci. 42, 298–309.

Dimitrovova, Z., Advani, S.G., 2002. Analysis and characterization of relative permeability and capillary pressure for free surface flow of a viscous fluid across an array of aligned cylindrical fibers. J. Colloid Interf. Sci. 245, 325–337.

Foley, M.E., Gillespie, J.W., 2005. Modeling the effect of fiber diameter and fiber bundle count on tow impregnation during liquid molding processes. J. Compos. Mater. 39, 1045–1065.
Gebart, B.R., 1992. Permeability of unidirectional reinforcements for RTM. J. Compos. Mater. 26, 1100–1133.
Lucas, R., 1918. Veber das Zeitgesetz des kapillaren aufstiegs von flussigkeiten. Kolloid Z. 23, 15–22.
Pillai, K.M., Advani, S.G., 1995. Numerical and analytical study to estimate the effect of two length scales upon the permeability of a fibrous porous medium. Transport Porous Med. 21, 1–17.
Pillai, K.M., Advani, S.G., 1996. Wicking across a Fiber-Bank. J. Colloid Interf. Sci. 183, 100–110.
Potter, K., 1997. Resin Transfer Moulding. Chapman & Hall, London.
Washburn, E.W., 1921. The dynamics of capillary flow. Phys. Rev. 17, 273–283.
Young, W.-B., 2004. Capillary impregnation into cylinder banks. J. Colloid Interf. Sci. 273, 576–580.